Engineering Science and Technology, an International Journal 49 (2024) 101597

Contents lists available at ScienceDirect

Engineering Science and Technology, an International Journal

journal homepage: www.elsevier.com/locate/jestch

The impact of force equalization in minimizing the effect of drift in feedback transducers in torque-summed electromechanical actuators

Fawaz Y. Annaz

Birmingham City University, The School of Engineering and the Built Environment, Millennium Point, Curzon Street, Birmingham B4 7XG, United Kingdom

ARTICLE INFO

Keywords:
All-electric aircraft
Electromechanical actuators
Force equalization
Torque summing architecture
Force fight

ABSTRACT

This paper focusses on implementing force equalisation to reduce or eliminate torque disparities in a four-lane torque-summed electromechanical actuator that drives the inner board aileron control surface on the Sea Harrier aircraft. Proportional, integral, and derivative control action achieved position control of the common output shaft, following two failures. The analysis included the effect of inherent motor disparities and drift in feedback transducers. Three-phase motor models were considered to account for the influence of the inherent torque ripple effect, and the influence of inertial and aerodynamic loads over various flight envelopes were also included in the analysis. Simulation tests demonstrated that although torque disparities between mismatched lanes are influenced by drift in potentiometer readings, force equalization was proven to be effective in eliminating such deviations.

1. Introduction

The first flight took place in 852 when Abbas ibn Firnas (wearing loose cloak that was stiffened with wooden struts) jumped from the minaret of the Great Mosque of Cordoba. His fall was not entirely successful, but it was slow enough that he managed to walk away with minor injuries. His attempt marks an example of the earliest parachute jumping [1]. Thirty-five years later (in 887, and at the age of 70), he successfully flew for 10 min after leaping from a cliff in an unpowered machine that was made of silk and eagle feathers, thus achieving the first unpowered man-carrying machine [1,2].

One thousand years later, the Wright Brothers started experimenting with gliders, where they successfully demonstrated that a glider of large surfaces could be easily controlled by manipulating the surfaces rather than moving the body of the operator. Following many tests and consultations with other engineers (such as Octave Chanute, who was also experimenting with unpowered flights), the brothers were successful (in 1903) to fly the first self-powered man-carrying machine. In these flights, they manipulated surfaces via hand and feet control leverages [3,4,5].

Manual pilot manipulation of control surfaces (via cables, pulleys, joints, and rods) remained throughout the development of early aircrafts. However, as airframes and control surfaces developed and the number of control surfaces increased, hydraulic actuators were introduced to generate the demanded forces to move the control surfaces. This introduced nonlinearities such as stiction, friction, and hysteresis which affected the handling quality. To improve this, the Fly-by-Wire concept was introduced, where pilot inputs are electrically sensed to activate hydraulic actuators to move the various control surfaces.

This modification dictated that aircrafts had to include two power sources (hydraulic and electric), reducing their reliability to those of the onboard hydraulic systems. To increase reliability and to consolidate power sources into one, the concept for the all-electric aircraft was born. This need, along with the development of high-density servo motors, power electronics, and digital control technologies, novel actuation systems, such as electrohydraulic actuation (EHA) and electromechanical actuation (EMA) systems.

In recent years, EMA systems have gained wide recognition and are gradually replacing EHA. This is because they pose significant weight reduction, cost savings, better overall energy efficiency, and improved reliability and maintainability [6,7]. To meet the accepted fail-operational/fail-safe requirement, smart EMA systems had to be designed with architectures that offer (at least) the same reliability of the dual-tandem EHA systems that they are replacing [8,9,10,11,12].

To contribute to the ongoing research activities in the all-electric aircraft concept, the EMA architecture (shown in Fig. 1) was initiated at Queen Mary University of London. The design comprises of a four lanes actuation system driving a common output shaft via a torque-summed gearbox assembly. In this design, the actuator was assumed to experience one failure at a time, where failures could be due to single or repeated motor or feedback transducer (FBT).

E-mail address: fawaz.annaz@bcu.ac.uk.

https://doi.org/10.1016/j.jestch.2023.101597
Received 1 September 2023; Received in revised form 29 November 2023; Accepted 10 December 2023
Available online 30 December 2023

List of Symbols

M	Mach number $0.2 \leq M \leq 1.0$
Pot_n	Potentiometer reading on motor "n"
T_L	Total developed torque
Tac_n	Tachometer reading on motor "n"
T_o	Output torque
T_{q_n}	Torque due to lane n
ΔT_{np}	Torque disparity between lanes n and p
T_{A_v}	Variable aerodynamic component
T_{A_s}	Steady aerodynamic component
$\alpha_G{}^o$	Angle of incidence
$\delta_a = \pm 18^o|_{M=0.2}$	Aileron deflection $\pm 18^o$ during low aircraft speed
δ_z	Zero net-aerodynamic angle
φ and $\dot{\varphi}$	Aircraft bank angle and roll rate

*Abbreviations: performance.**

FF	Force Fight
FE	Force Equalization
FBT	Feedback Transducer
TD	Torque Disparity
EMA	Electromechanical Actuator
Pot	Potentiometer
$Systems\|_{Tmax^{\pm}}$	Systems operating in the $T_{max^{\pm}}$ modes
FDI	Fault Detection and Fault Isolation System.
MVAD	Monitoring Voting Averaging Device

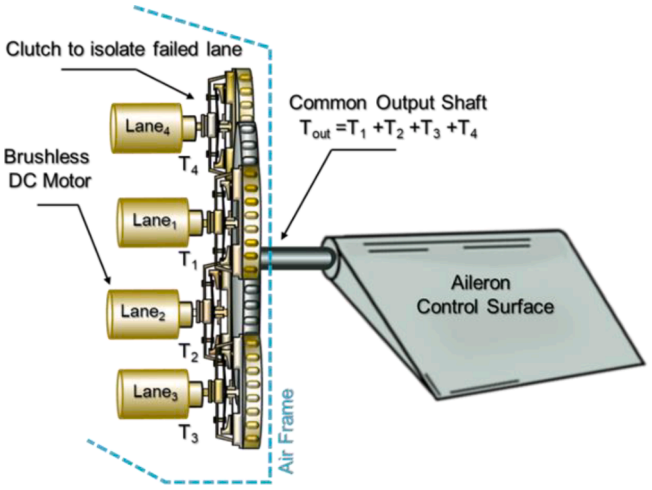

Fig. 1. The proposed electromechanical architecture.

The author in [13] demonstrated that motor failures (when compared to failures in tachometers or potentiometer) had the largest impact on the actuation system response and hence the aircraft response in roll. To safely detect, identify and isolate failures the system also includes an embedded fault detection and fault isolation (FDI) system. Once a failure is detected the FDI system sounds an alarm, and the faulty component is isolated. In the event of a motor failure, in addition to electrically isolate the motor, a clutch is activated to physically disconnect the faulty motor.

The main aim of this paper is to examine the effectiveness of force equalization (FE) in reducing or eliminating torque disparities (TDs) between inherently mismatched motors, and to assess the effect that drift in feedback transducers (FBTs) readings has on the overall performance.

2. Redundancy in the all-electric aircraft

Over the years, several studies have emerged and led to the development of programs that assessed electromechanical actuator systems survivability, vulnerability, fault tolerance, and power consolidation, addressing the benefits of the all-electric aircraft concept for the next generation fighters [14,15,16]. Many of these studies have compared and cross-examined hydraulic and electromechanical actuators (EMA).

One of the early studies that examined mismatched inputs mechanizations was presented in a comprehensive report by NASA [17]. Fig. 2a shows the Parallel/Active mechanizations, with the three available (force, velocity, and position) summing options. This configuration incorporates multiple channels that perform identical control functions simultaneously. In force summing, the common output force is equal to the sum of the individual contributed forces. Here, the individual lanes are force voted to achieve an output that represents the mid-value of all input commands. Thus, force fight is possible, if there is a mismatch in the commanding input or the characteristics of the lanes. In the velocity summing systems, the output velocity and output force are the average sum of the individual lanes contributions. Therefore, there will be no force fight problem in this type of architecture. Similarly, position summing systems will not incur any force fight at the output, as the net position is the average contribution of the individual inputs. However, in this architecture, linkages will restrict the output stroke capability after a channel failure or a channel shutdown. Therefore, in the position summing architecture individual actuators must be able to achieve larger strokes to accommodate for the loss of any of the lanes.

The other configuration that was described by the authors in [18,19] is the active/standby configuration, as shown in Fig. 2b. In this architecture only one-channel controls the output of the system at any one time. Therefore, in this configuration: Control channels operate independently, however, in the event of a failure of an active control channel, a rapid transfer to an operating standby channel is essential to avoid degradation.

The authors in [20] presented an invention that provides a structurally redundant control surface actuator that tolerated dormant failure and catered for dual failures in mechanical, hydraulic or a combination of both, without disconnecting from the control surface, as shown in Fig. 3. The actuator meets the system specification and safety standards, and it proposes an architecture that does not require balance weights with negligible 'force contention' between the output forces. This was achieved by eliminating balance weights from the control surfaces and installing three parallel actuators. These actuators would usually experience force fight along the control surface, which could result in structural damage and ultimate failure. However, to reduce such force contention the author proposed the addition of computer monitored pressure sensors to closely align the actuators positions. The author also pointed out the following two alternatives: 1) An expensive rudder control, which utilises a three parallel actuators configuration that are controlled by common three hydraulic valves; and 2) a computer monitored dual simplex actuators (to each surface) method which is more suitable for aircrafts with fly-by-wire capability.

3. Prior arts addressing force fight (FF) in redundant actuation systems

Although many studies have described torque-summed architectures, very few have addressed the possibility of FF between the redundant lanes. It is the aim of this section to present prior arts that have addressed the FF concept by exploring various redundancy modes

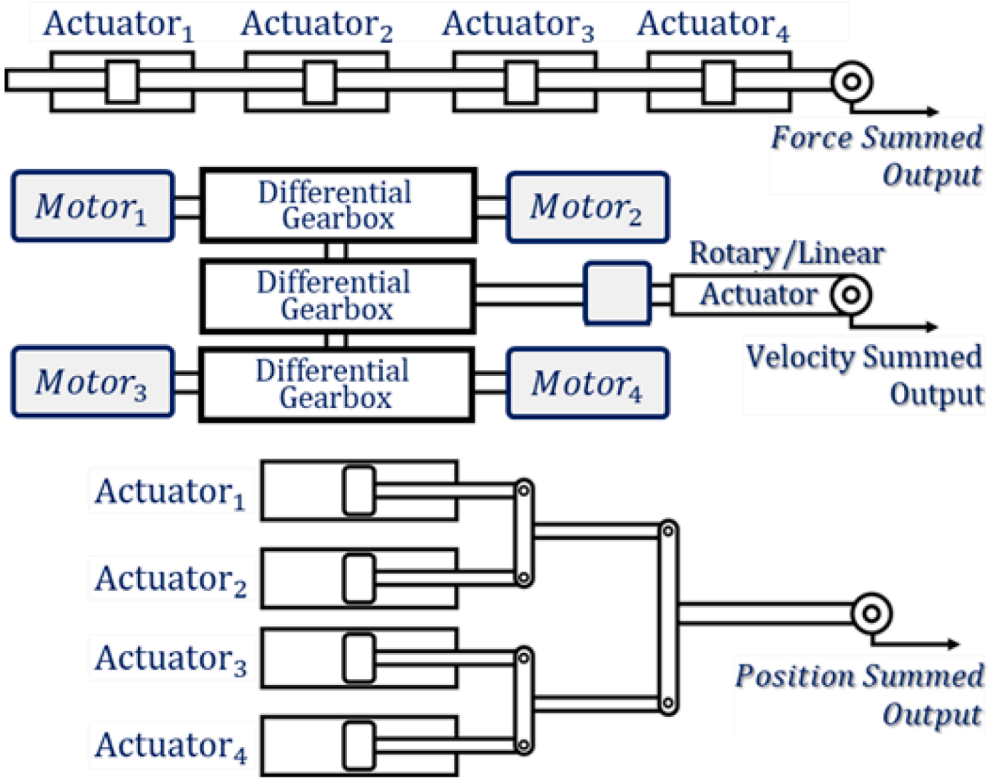

a) Parallel/Active Configuration

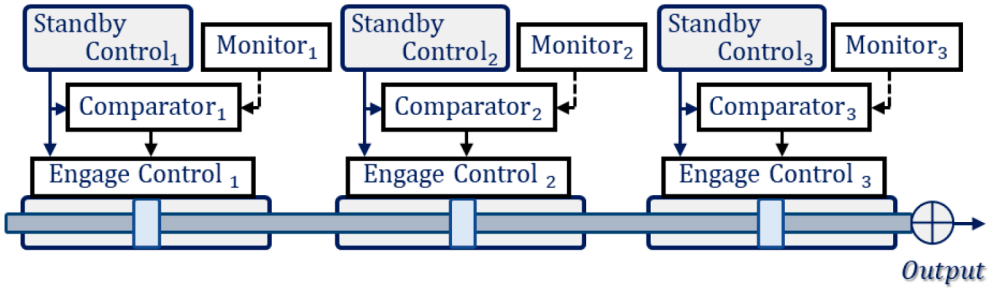

b) Parallel/Active Configuration

Fig. 2. A view of a dual hydraulic cylinder multiple tie rod system [10].

and assessing alternative control strategies to hybrid solutions.

The authors in [21,22] presented the consolidation of more than a channel through the deployment of parallel hybrid (i.e., Hydraulic and Electric) systems in active/passive and active/active redundancy modes. In the active/passive mode range, only a single actuator operates and there will not be any force fight between the consolidated lanes. However, in the active/active mode range, the actuators function at the same time. Thus, control surfaces that are driven by multiple actuation systems are likely to experience force fighting effect. This has dangerous effects on the aircraft system as it is possible to generate tracking accuracy errors and damage the control surface [23]. Therefore, force fighting has become a trending research area in aircraft actuator systems design. Good examples of such approaches include the work presented by the authors in [24,25,26], who investigated suitable control strategies to redundant actuation systems with hybrid solutions to achieve static FE.

The authors in [24] investigated suitable control strategies in redundant hybrid-actuation systems, to achieve static FE, as shown in Fig. 4. The performance of a virtual redundant actuation test bench was verified against experimental results. The testbed evaluated the cause of static force fighting in three different FE control strategies, namely: a) Position control of a combination of servo-hydraulic and electromechanical actuators, with FF signals compensated position feedback signals by tuning the position sensors offsets, as shown in Fig. 4a; b) Force control of a combination of servo-hydraulic and electromechanical actuators, with motor current control achieved faster control response, as shown in Fig. 4b; c) No-load control of a combination of servo-hydraulic and electromechanical actuators, with FF cancellation as the EMA did not have direct influence on the load position, as shown in Fig. 4c.

The authors in [25,26] have further proposed FE control strategies to a hybrid (electrohydraulic and Electromechanical) actuation system that drove a single aileron control surface. The study considered a parallel summing arrangement of the electrohydraulic and the EMAs, where it confirmed the significant effects of the strategies on static FE and proposed that future work should focus on dynamic FE. The authors prevalidated two strategies: initially on a virtual test bench, and then

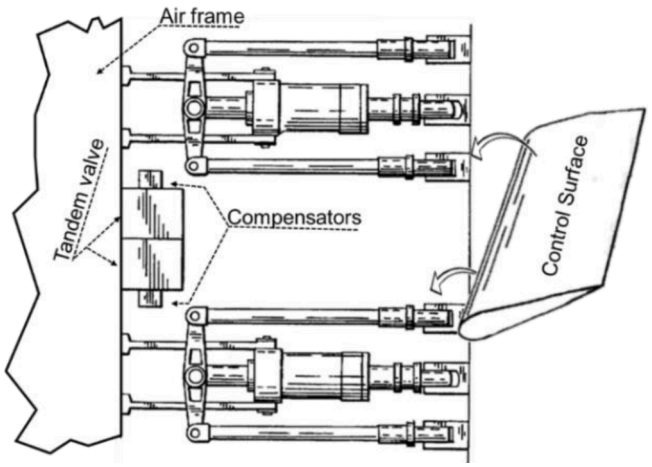

Fig. 3. An orthographic view of a dual hydraulic cylinder multiple tie rod system.

experimentally. The first is to integrate FF signals to compensate position control; and the second is to operate in master/slave modes. One main drawback in this work is the fact that the study did not consider the consolidation of power sources as it utilised hydraulic and electric, as shown in Fig. 5.

The author in [27] assessed the suitability of a passive electromechanical test rig in reproducing the dynamics that EMAs might experience in various aerospace applications. Although the rig omitted some of the effects that an actuator might experience in flight, it included most of the impactful characteristics that are important for the early phases of testing. The author in [28] replicated a spring-mass-damper test rig to capture first order flight system response, where it was reported that a linear model can reproduce very accurate characteristics. The author reported that the approach could be expanded to assess FF in several EMAs on future aerospace vehicles.

The authors in [29] stated that in most cases primary flight control systems on commercial airliners are configured in parallel force or position summing configurations. When operating in an active/active mode, parallel force summing configurations will result in serious force fighting between actuators, which must be addressed. However, parallel position summing configuration will not result in force fighting, and it is suitable for all kinds of actuators [19,29]. The authors also proposed position synchronization for hybrid electromechanical actuation systems.

Similarly, Rehman et al have taken the redundancy concept a step further and argued that higher reliability can only be met by the inclusion of dissimilar redundant system to avoid common failure modes [30]. The authors gave the example of the actuation system on the A380, which is shown Fig. 6 and comprises of two actuation networks, namely electric and hydraulic. However, although higher reliability can be achieved in such systems, control surfaces that were driven by manipulators with different driving principals experienced FF, as the manipulators were rigidly connected. To solve this FF issue, model reference adaptive control was proposed to synchronize the motion of the conventional hydraulic actuation system and EHA system. It was reported that performance improvement was achieved with some oscillatory behaviour due to high gain adaptation.

It is the aim of this paper to present and evaluate force equalisation on a single-type mismatched torque-summed (four-lanes) architecture, shown in Fig. 1. The impact that drift in FBTs has on force fight between lanes will be assessed. This system was initially investigated by the QWM Avionics group, and detailed design specification, architecture consideration, cross monitoring and threshold setting techniques, along with different levels of modelling complexity maybe found in [13,31,32].

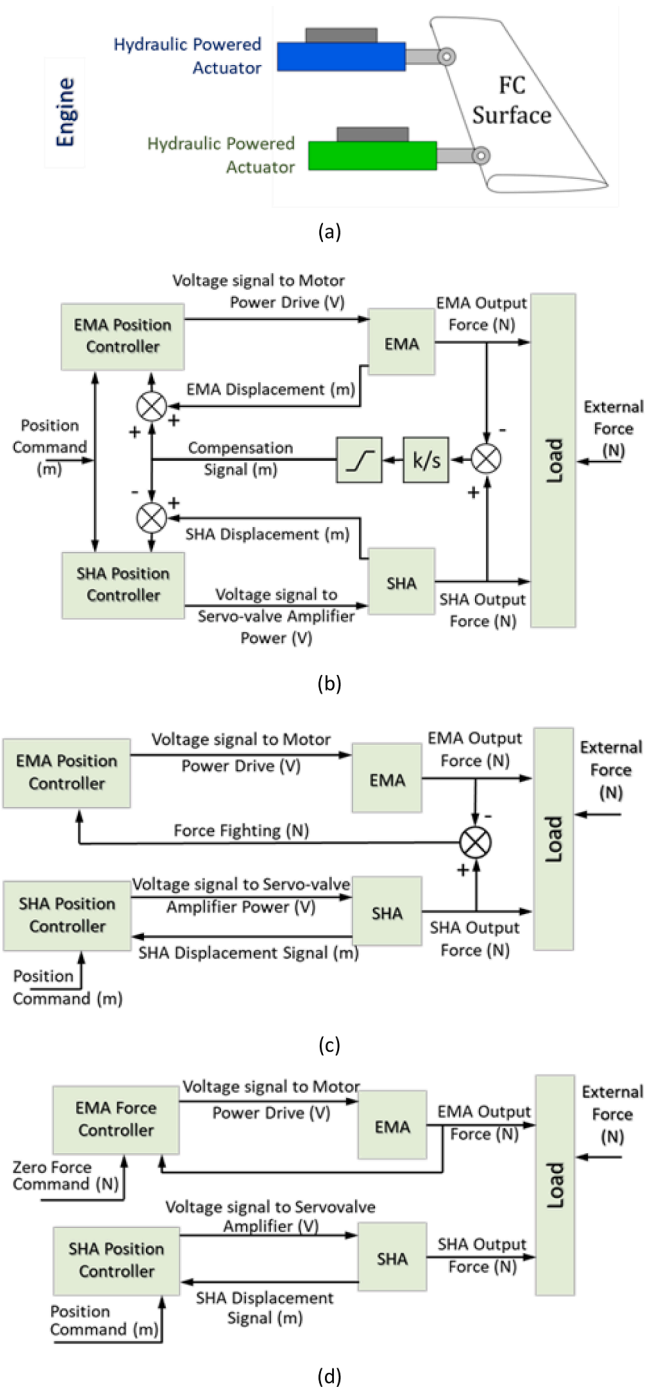

Fig. 4. Hydraulic & electric hybrid actuation system.

The main drawbacks in the above studies are: 1) they did not consider power consolidation of power sources; and 2) they did not consider and did not assess the impact of drift (or failure) in feedback transducers on force-summed architectures. Therefore, the aim of this paper is to assess the impact of such deviation in feedback transducers on force fight between mismatched lanes in a four-lanes electromechanical actuation system.

4. System under consideration

The system shown in Fig. 1 was designed to meet the imposed fail-operational/fail-safe requirement [8], by including redundancy in the driving channels and FBTs. The actuator comprised of four torque-

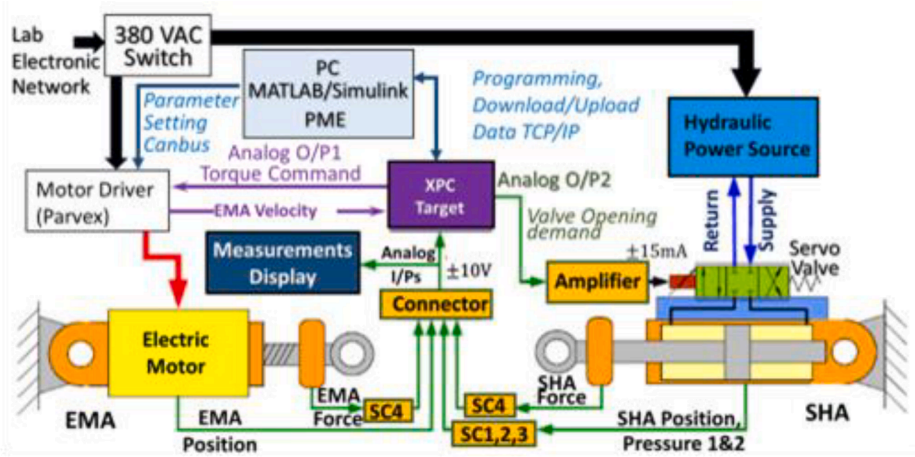

Fig. 5. Control system schematic of test bench.

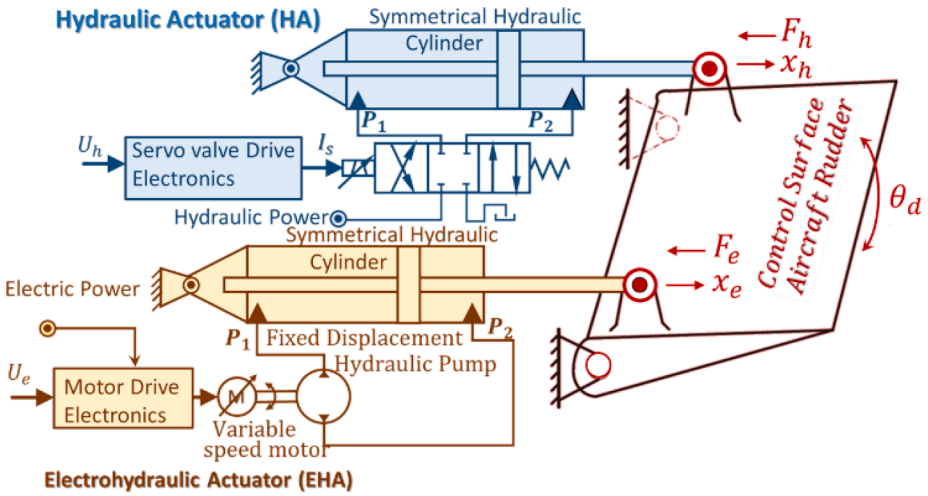

Fig. 6. Redundant actuation system with adaptive control [30].

summed lanes of brushless dc motors to deliver the necessary output torque to overcome inertial and aerodynamic loads that act on the control surface that it is driving. The lanes were assumed to contain their own microprocessor/s to control and monitor the actuator for (motor and FBT) failures over a wide range of flight envelope for aircraft speeds in the range $0 \leq M \leq 1.0$.

As the resultant driving torque equals the algebraic sum of the individual torque contributions, previous studies raised concerns about the likelihood of FF between the lanes because of the differences in motor parameters and FBTs. In this study, the effectiveness of FE to minimize the effect of the inherent mismatch between lanes; and unnoticed drift in transducers readings will be investigated. Fig. 7 is a block diagram of the closed control system, with and without force equalization. The shaded area in Fig. 7 corresponds to the FE control scheme as the (position and velocity) feedback signals equal to the averaged readings from the monitored redundant potentiometers and tachometers. On the other hand, the unshaded portion of the figure corresponds to the scheme without force equalization, with independent position and velocity feedback signals. In both schemes, both potentiometers and tachometers are monitored for failures before they are fed back to the individual controllers.

As all the lanes are locked together via a gearbox to drive the common shaft: a) the output torque will be the total sum of the torques contributed by the individual lanes; b) the output shaft position and speed will be the same as those of the individual lanes; c) therefore, it is irrelevant where the feedback sensors are placed; d) however, it is important to realise that isolation (of a potentiometer or a tachometer) after a failure will not necessary result in the isolation of the whole lane if the motor built in transducers are used; e) motor isolation (following a failure) will result in an immediate loss of the built in transducers; f) therefore, a combination of the motor-built in and external transducers will be a better option (but this depends on the application, cost and housing capacity). Regardless of the approach adopted, designs should conform to actuation and aircraft military standards [33,34].

5. The control surface position control system

A proportional and integral (PI) action controller with velocity feedback was employed to cater for any load nonlinearities and to modify the open loop poles, so that the loci pass through dominant complex poles. Thus, the controller was designed to maintain relatively constant undamped natural frequency with slight drop in the damping factor, ζ. Full treatment of the control system design maybe found in [13,32], where it is demonstrated how the actuator time and frequency responses specification were met along with the aircraft response in role. The design specifications are as follows:

Actuator Design Specification: Operating over a flight envelope of $M = 0 \sim 1$, the actuator was designed so that it: 1) can provide maximum rotary outputs of $\pm 18^o$. 2) operates with maximum aileron authority limits of $\delta_a = \pm 18^o$ (at low aircraft speeds) and $\delta_a = \pm 2^o$ (at high aircraft

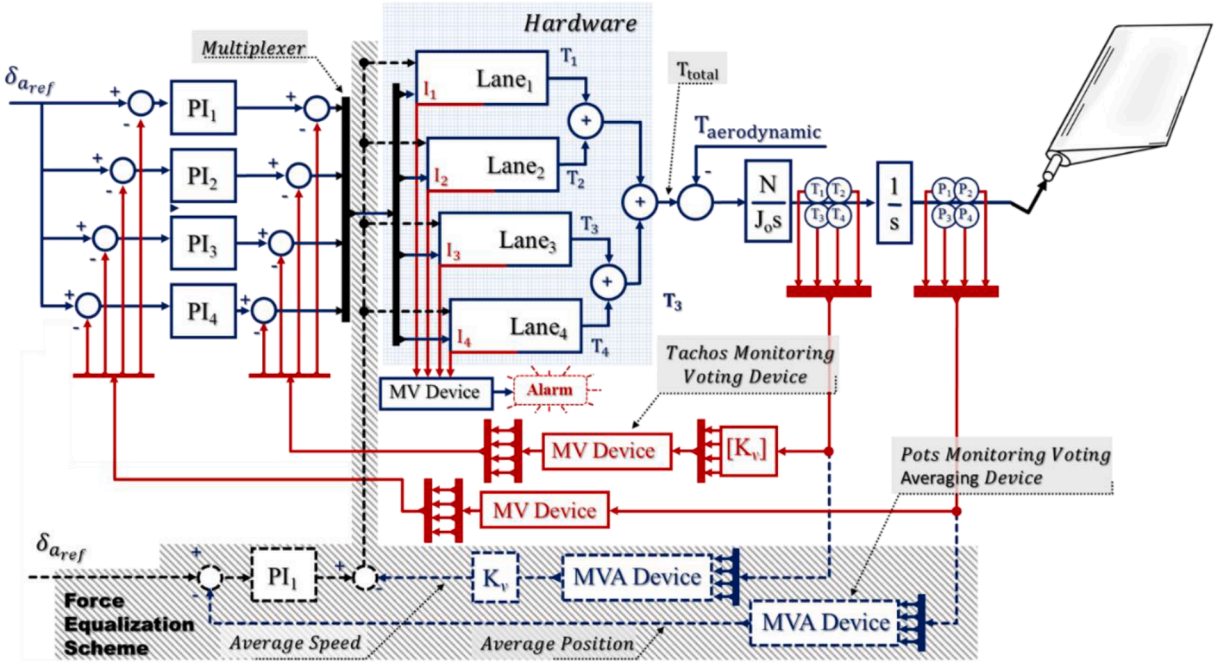

Fig. 7. A Torque-Summed Architecture with (shaded area) and without FE schemes.

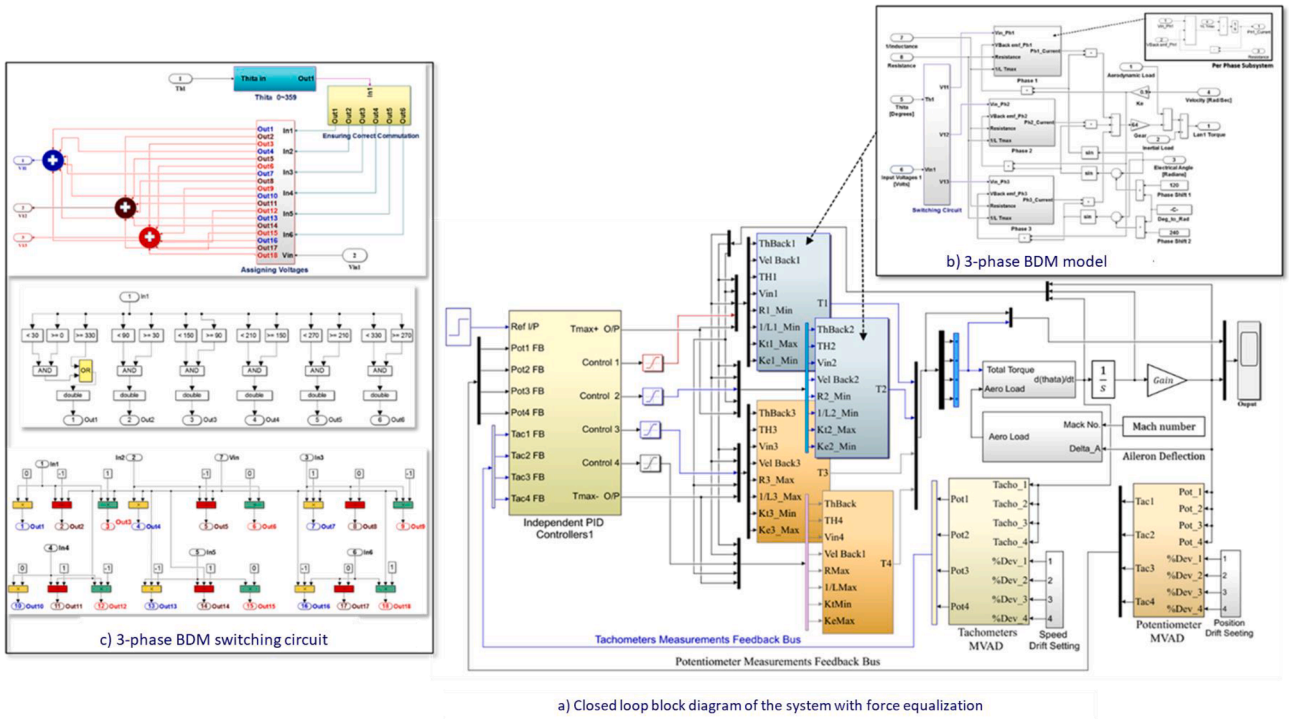

Fig. 8. Closed loop block diagram of the system without the force equalization scheme.

speeds) with linear variation at intermediate speeds. 3) has a minimum output rate of $0.5\,rad.s^{-1}$. 4) has a bandwidth of 8 Hz at 1^o (based on -3 dB at 5 % of maximum output amplitude). 5) can overcome inertial and aerodynamic loads (after two failures) of a control surface similar to the inner-board aileron on the Sea Harrier. 6) has a first nuisance disconnects probability under 10^{-4}.

The Aircraft Response in Role Specification: Transients following the isolation of one or two lanes will result in: 1) maximum aircraft manoeuvre of $+5.0g$. 2) maximum bank angle of $\varphi = 3^o$. 3) maximum roll rate of $\dot{\varphi} = 5^o s^{-1}$ [33,34].

The Simulink closed loop block diagrams of the proposed actuator are shown in Figs. 8 and 9. Fig. 8 shows the system without the force equalization scheme, and Fig. 9 shows the system that deploys force equalization scheme. Although both schemes include the 3-phase brushless dc motor models and the necessary switching circuits, the subsystems are shown in Fig. 8 only. The Simulink models also include the aerodynamic and inertial load models. The inertial load was proven to be proportional to the maximum sinusoidal authority limit

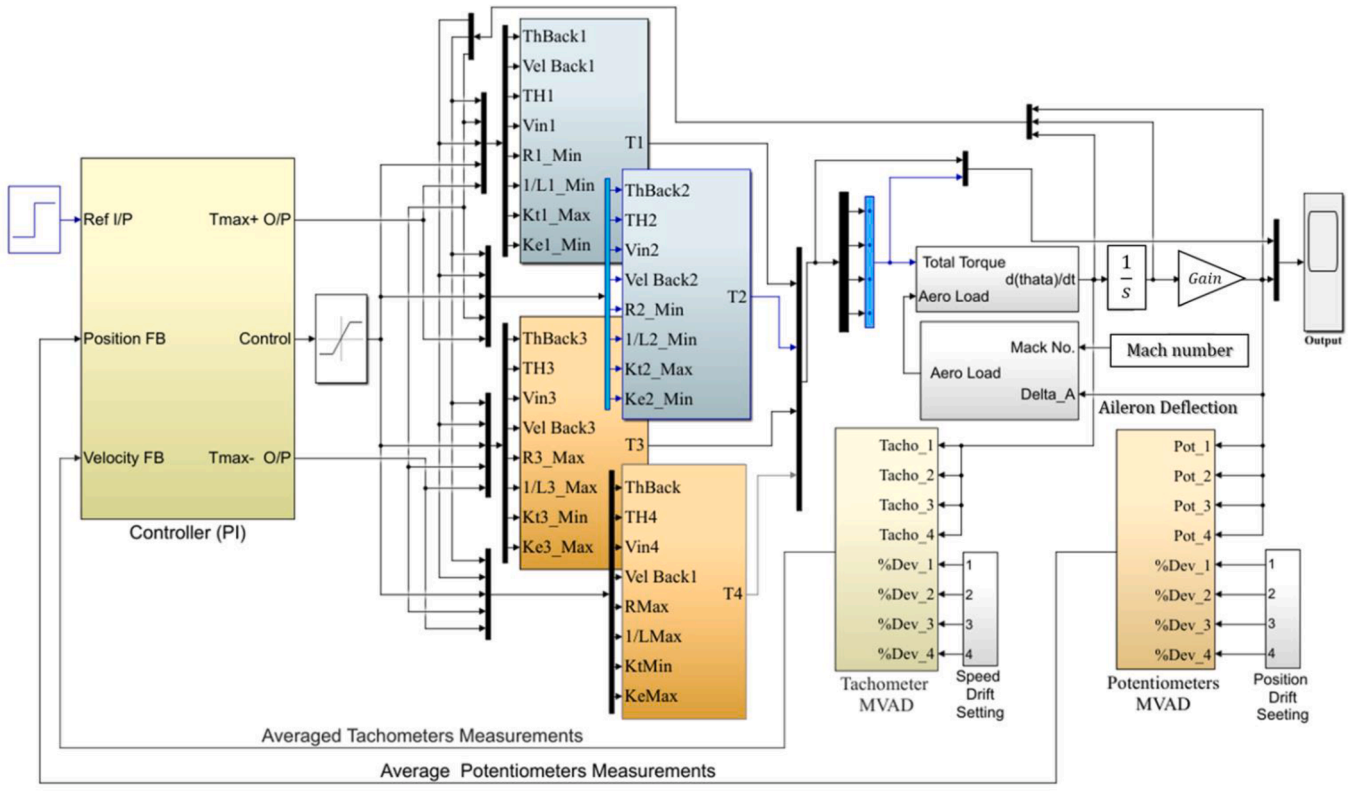

Fig. 9. Closed loop block diagram of the system with the force equalization scheme.

excursions, and that the $\delta_a = \pm 18^o|_{M=0.2,\,8Hz}$ flight condition generated the maximum inertial load. The variable aerodynamic component (T_{A_v}) was shown to be aileron-deflection and aircraft speed dependent, however, the steady component (T_{A_s}) depends on the aircraft speed only and is constant over the two aileron surfaces. For this configuration, the resultant loads (T_L) will typically be in the range $240Nm \leq T_L \leq 5714Nm$ [31].

Position control was achieved through two PID configurations, with the main differences between the two are the controller and the monitoring devices. The first scheme (Fig. 8) implements individual control channels, where each of the lanes contains its own controller that utilise feedback signals from each of the redundant transducers. The second configuration with FE (Fig. 9), utilises a common controller that drives all channels with the fed back signals being the average measurement of the redundant healthy/active transducers.

The motors were assumed to have parameters with the following nominal and tolerance values: Resistance, $R = 7.2 \pm 12\%\,\Omega$; Inductance, $L = 17.7\text{x}10^{-3} \pm 30\%$ H; Torque constant, $K_t = 1.0 \pm 10\%$ Nm/A; and Voltage constant, $K_v = 1.0 \pm 10\%$ V/(rad/sec). Therefore, motors could deliver torques within the range $T_{max^-} = 19.35Nm \leq T_{max^\pm} \leq 30.11Nm$, [35,36]. To assess the effectiveness of FE, the analysis assumed motors to be operating within the two extremes, so that: $Lanes_{1\ and 2}$ delivering the higher band of peak torques"T_{max^+}"; and $Lanes_{3\ and\ 4}$ delivering the lower band of peak torques "T_{max^-}". Operating in these modes will be referred to as $T_{max^\pm}$, as summarised in the expression below:

$$\begin{aligned} T_1 = T_{1^+}; T_2 = T_{2^+} = T_{max^+} \\ T_3 = T_{3^-}; T_4 = T_{4^-} = T_{max^-} \end{aligned} \quad (1)$$

Although typical FBTs tolerances are in the range of ±0.7 2.3% [37,38], higher tolerances of 50 % and 100 % were considered. This is to: a) examine the effectiveness of FE on the TDs between mismatched lanes; b) verify the system performance; and c) assess the effect of undetected transducers drifts on the system response, where such high growth in measurement is associated with drift due to unnoticed

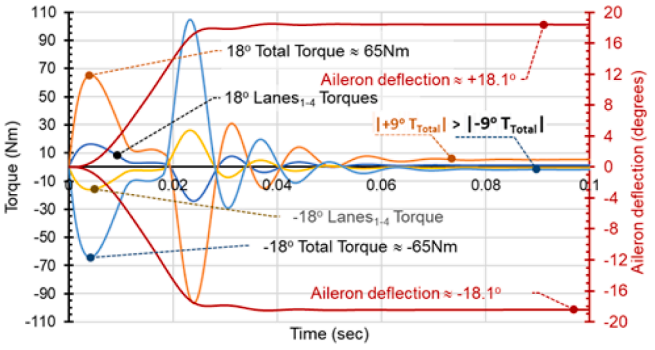

(a) $\pm 18^o$

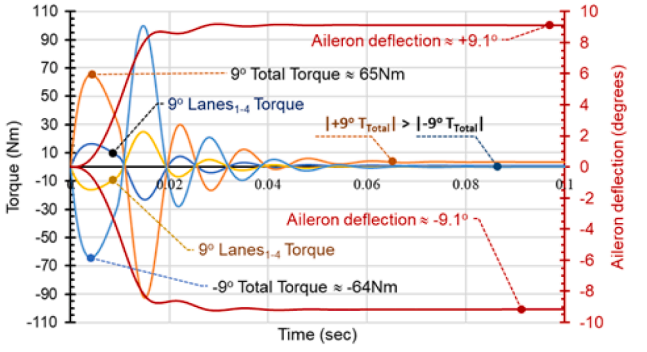

(b) $\pm 9^o$

Fig. 10. Individual and total torques as well as aileron deflection for an actuator with nominal motor parameter.

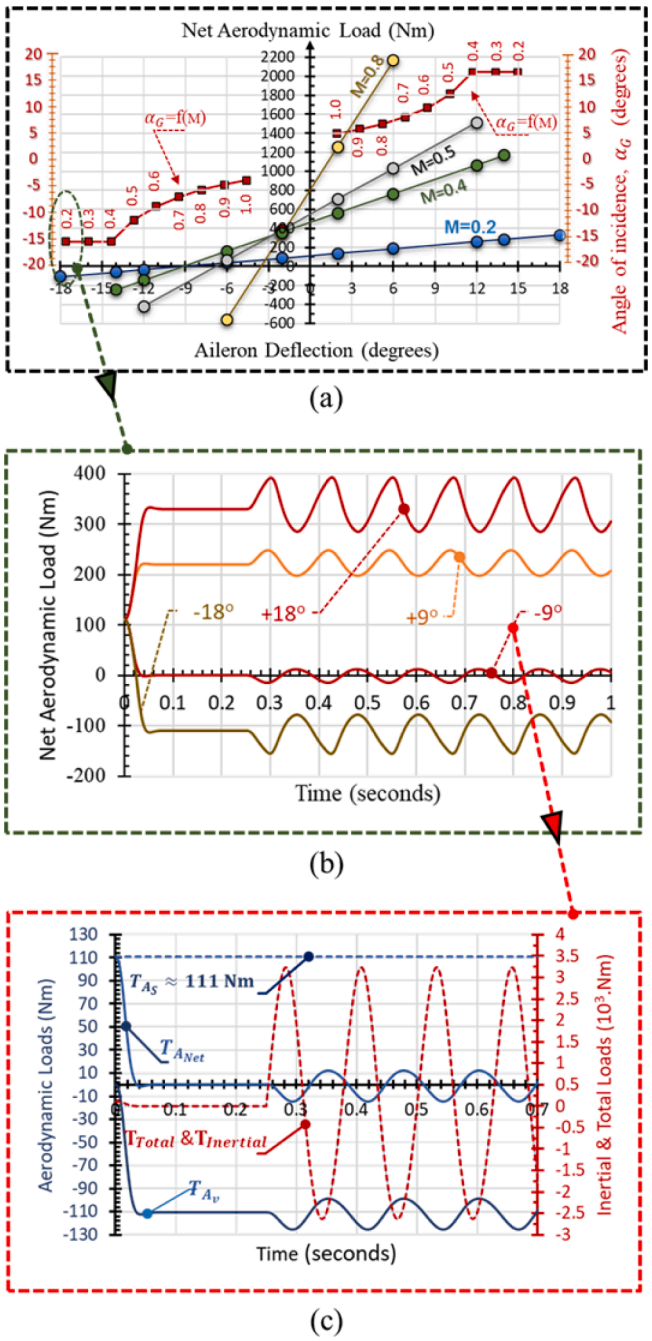

Fig. 11. Loads distribution in relation to aileron deflection and aircraft speed. a) Aerodynamic loads distributions for different flight cases b) Net-aerodynamic loads for $\pm 18^o|_{M=0.2}$& $\pm 9^o|_{M=0.2}$ c) Inertial and aerodynamic loads for $-9^o|_{M=0.2}$.

transducers failures.

6. Simulation test results

In this section, the impact of FE on reducing TDs between the lanes of the torque-summed architecture will be assessed. Simulation tests considered maximum loading over a wide range of flight envelopes (for aircraft speeds from M = 0.2 to M = 1.0) with aileron deflections at the maximum authority limits. However, mainly low-aircraft flight tests will be presented here, as it is at these regions force fight will be maximum.

The sequence in which the test results and analysis will be presented is as follows: Initially, the impact of FE will be assessed in systems with nominal parameters (Section 6.1). This is then extended (in Section 6.2) to assess the impact at regions where the aerodynamic load is zero (i.e., the acting loads are purely inertial). Then FE is assessed in actuators with highly mismatched lanes (I.e., maximum inherent TDs) with undetected (dormant) drifts in tachometers and in potentiometers feedback (Sections 6.3 and 6.4, respectively), where single and double dormant failure will be considered.

6.1. Force equalization in systems with nominal parameters

The impact of FE was first assessed on systems with nominal parameters, by examining the aileron position response, the individual torques ($T_{q_{1\ 4}}$) and total (T_{Total}) developed torques for various flight cases. During this study, the $\pm 18^o|_{M=0.2}$ and $\pm 9^o|_{M=0.2}$ were identified to be the key flight cases and are shown in Fig. 10. This is because the first case is when the actuator experiences maximum loads to achieve aileron deflections of $\pm 18^o$. The second case compares the system response at an angle where fluttering will take place. Section 6.2 will explain how these regions are identified over the flight envelop.

The simulation results in Fig. 10 show that all lanes reacted in a similar manner with the responses of the individual lanes being superimposed on each other. The responses due to $+9^o$ and $+18^o$ step inputs are the mirror image to those due to -9^o and -18^o step inputs; and all TDs were (as expected) equal to zero. Therefore, FE or its absence did not impact the response in nominal systems.

6.2. Force equalization at regions where the aerodynamic load is zero

The aerodynamic loads are made up of steady (T_{As}) and variable (T_{Av}) components, as shown in equation (2), where A and B are constants, α_G is the angle of incidence and $\overline{Q}(M)$ is the dynamic pressure. Clearly, T_{As} depends on the aircraft speed only, and T_{Av} depends on the aileron deflection and aircraft speed. This section assesses the impact of FE (on systems with nominal parameters) at regions where the net aerodynamic loads are zero ($T_{As} = -T_{Av}$).

$$\textit{Aerodynamic Load} = \begin{bmatrix} \textit{Steady Component} \\ (T_{As}) \\ A\ \alpha_G \end{bmatrix} \begin{bmatrix} \textit{Variable Component} \\ (T_{Av}) \\ +\ B\ \delta_a \end{bmatrix} \overline{Q}(M) \tag{2}$$

A wide range of flight cases were considered, and Fig. 11a shows the aerodynamic loads distribution for different aileron deflections and angles ($\delta_Z{}^o$) at which the aerodynamic loads are zero (for aircraft speeds of M = 0.2, 0.4, 0.5 and 0.8). For example, the aerodynamic loads were calculated for aileron deflections of -6^o, -3^o, 3^o and 6^o at M = 0.8 aircraft speed, and it was found that the angle at which the aerodynamic load was zero is at $\delta_Z = -3.5^o$ (which will be denoted as $\delta_Z|_{0.4} = -3.5^o$). The angles for other flight cases were also identified to be: $\delta_Z|_{0.2} = -9^o$, $\delta_Z|_{0.4} = -9^o$, and $\delta_Z|_{0.5} = -6^o$. Note that $\delta_Z|_{0.2} = \delta_Z|_{0.4} = -9^o$ because at these flight cases, α_G was limited to 15°, as shown by the two red (top) curves of Fig. 11a.

Then, the M = 0.2 flight case was considered to illustrate (as shown in Fig. 11b) the developed net-aerodynamic loads for reference inputs of $\pm 18^o$ and $\pm 9^o$. Fig. 11b shows the system response to step inputs of $\pm 9^o$ (for $t \leq 0.25$), and to additional sinusoidal inputs (of 0.5° magnitude at a frequency of 8 Hz) for $t > 0.25$. The figure clearly shows that for a reference input of $\delta_Z = -9^o$, the net-aerodynamic load remained to be zero, before it starts perturbing around zero Nm as the reference was varied between -9.5^o and -8.5^o.

Similar results were obtained for other reference angles, however, the net-aerodynamic load remained constant (not zero), before it started perturbing as the reference was sinusoidally varied at 8 Hz. As expected, the size of this perturbation varied, depending on the set reference input, however, in all cases: a) T_{As} added to the inertial load in one direction and opposed it in other direction; b) T_{Av} supported the inertial load in

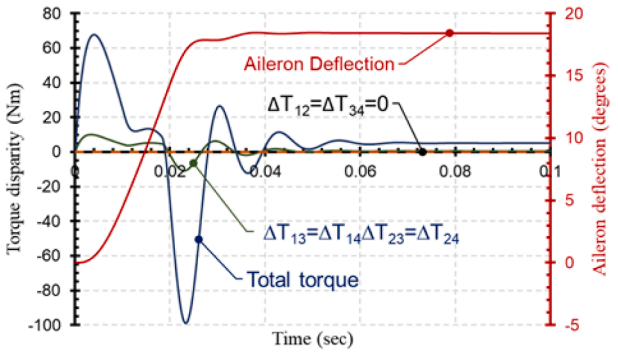

a) Responses with 0% drift in FBTs with (FE) and without FE ($\overline{FE}$)

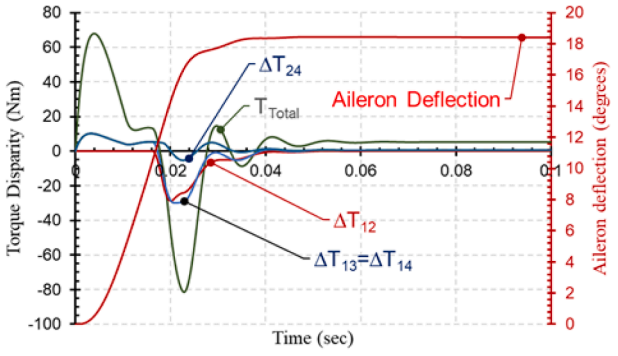

b) $\overline{FE}$ response with 50% drift on $Tachometer_1$ reading

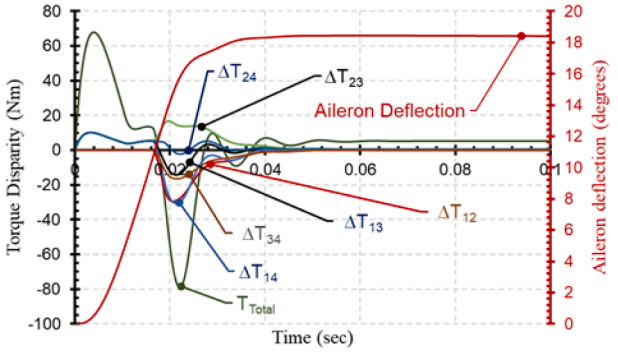

c) $\overline{FE}$ *response with* 50% drift on $Tachometers_{\ 1\&3}$ readings

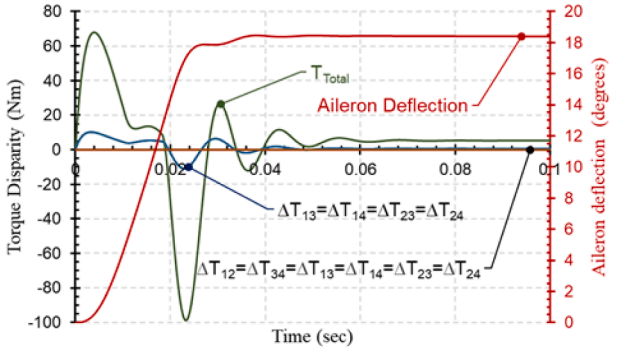

d) FE response regardless of drift percentage in one or more tachometers

Fig. 12. Position and TD responses of actuators operating in $T_{max^{\pm}}$ modes.

both directions.

With the actuator being designed to overcome high inertial loads, concerns over uncontrolled fluttering in the δ_Z regions maybe eliminated as the overall load contribution is significantly small, as shown in Fig. 11c. Therefore, δ_Z regions do not cause concern, will not be considered in the next analysis and discussions.

6.3. *Force equalization in* actuation systems$|_{\text{Tmax}^{\pm}}$

Actuation systems$|_{\text{Tmax}^{\pm}}$ are (as mentioned in Section 5) actuation systems that include mismatched motors that are operating in the $T_{max^{\pm}}$ modes that yield inherent torque disparities. Here, $Lanes_{1\text{ and }2}$ were assumed to be operating at $T_{max^{+}}$, and $Lanes_{3\text{ and }4}$ were assumed to be operating at $T_{max^{-}}$, (i.e., $T_{q1} = T_{q2} = T_{max^{+}}$ and $T_{q3} = T_{q4} = T_{max^{-}}$). The next sections will examine the impact of force equalization on such systems in the absence and presence of drift in feedback measurements.

6.3.1. *Impact of FE on* actuation systems$|_{\text{Tmax}^{\pm}}$ *without drift in feedback measurements*

Here, the response of actuation systems$|_{\text{Tmax}^{\pm}}$ that implement force equalization (With-FE) is compared those that do not implement force equalization (Without-FE). The architectures were assumed to be operating in the $T_{max^{\pm}}$ modes, with no drift in their feedback measurements.

As expected, Fig. 12a shows the response of the two architectures to be identical, with initial torque disparities (ΔT_{13}, ΔT_{23}, ΔT_{14} *and* ΔT_{24}) that rapidly reduced to zero. The figure also shows that force equalization did not impact the actuator position response, and aileron deflections of 18.4^{o} were achieved in both cases. This is logical, as FBTs were assumed not to suffer from any drift in their readings, hence the individual control signals ($control_{1,2,3\text{ and }4}$) in Fig. 8 equal the common control signal in Fig. 9.

6.3.2. *Impact of FE on* actuation systems$|_{\text{Tmax}^{\pm}}$ *with drift in tachometer measurements*

Here, the impact of force equalization is assessed with the actuator operating in $T_{max^{\pm}}$ modes, and with the tachometers experiencing various degrees of drift in their measurements. Simulation tests with a wide range of drift were considered. However, as examples only simulations tests that consider 50 % drift on one and two tachometers are shown in Fig. 12b, 12c and 12d. The plots in Fig. 12b and 12c are for tests without FE (i.e., $\overline{FE}$); and those in Fig. 12d are for tests when FE being implemented. All the results assessed the aileron deflections in the $18^{o}|_{M=0.2}$ flight case.

Fig. 12b shows the aileron responses when the tachometer in $Lane_1$ only experienced 50 % drift in its measurement. Although it is highly likely for tachometers to have tolerances more than 2.3 %, higher order deviations were considered to simulate dormant failures (i.e., failures that went unnoticed by the FDI system). This is to easily visualise the effect of FE and to understand the impact of unnoticed dormant drift in tachometer readings on the system behaviour.

The results show that in the absence of FE (i.e., $\overline{FE}$) and drift in $Tachometer_1$ readings will result in larger torque disparities between $Lane_1$ and $Lane_2$ (ΔT_{12}); and $Lane_1$ and $Lanes_{3\text{ and }4}$ (*i.e.*, $\Delta T_{13} = \Delta T_{14}$), as shown in Fig. 12b. Drift in the readings of two tachometers (i.e., $Tach_1$ and $Tach_3$) will result in torque disparities between all the lanes, as shown in Fig. 12c.

However, systems that implemented FE, the disparities remained constant regardless of the drift percentage and the number of lanes affected, indicating the limited effect of drift on torque variation, as shown in Fig. 12d. In fact, the response in Fig. 12d is very much resembles that of Fig. 12a (where 0 % drift was assumed in FBTs). This is expected, as FE utilises a common control law with averaged fed back signals.

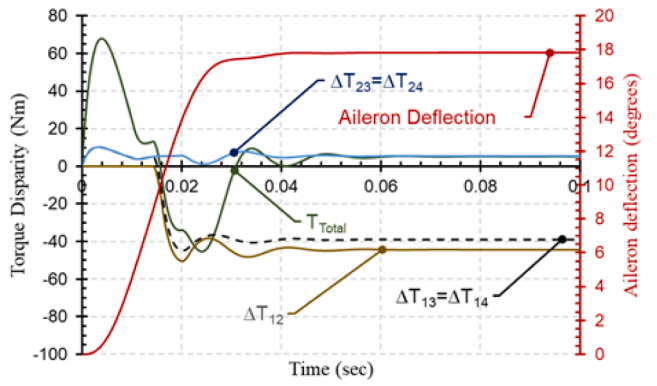

a) $\overline{FE}$ response with 50% drift on Pot_1 reading

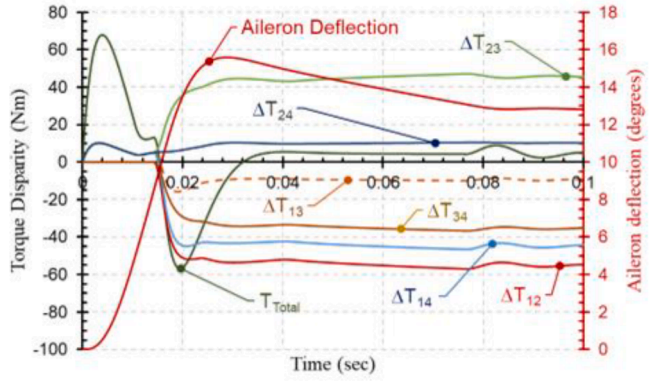

b) $\overline{FE}$ response with 50% drift on $Pots_{1\&3}$ readings

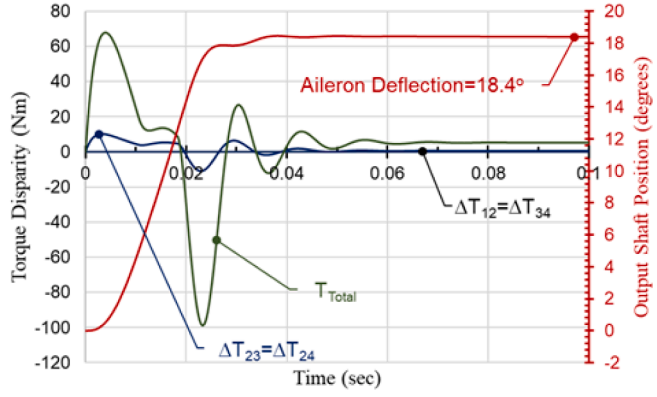

c) FE response regardless of drift percentage in one or more potentiometers

Fig. 13. Position and TD responses due to drift in potentiometer readings.

6.3.3. Impact of FE on actuation systems$|_{Tmax^{\pm}}$ *with drift in potentiometers measurements*

Here, the impact of force equalization is assessed with the actuator operating in Tmax$^{\pm}$ modes with various degrees of drifts in its potentiometer's measurements. Here again, although simulation tests with a wide range of drift were conducted, Fig. 13 shows only tests that demonstrates the effect of 50 % drift on one and two potentiometers will be presented (for the $18^{o}|_{M=0.2}$ flight case).

The first two plots in Fig. 13 are the responses of systems without FE (i.e., $\overline{FE}$); and the last plot (Fig. 13c) shows the response of a systems that implemented FE. Again, here the percentage drifts have been exaggerated to simulate unnoticed drifts to assess the impact of FE and compare it to $\overline{FE}$.

Fig. 13a shows the result for a test that assumed 50 % drift on the reading of the potentiometer in $Lane_1$ (i.e., Pot_1). The drift resulted in: a) the slowdown of the other lanes, so that the output shaft position reached the set demanded input (aileron deflection of 17.8^{o}); b) the resulting torque drop in $lane_1$(*i.e.*, Tq_1) was compensated by the other lanes, hence increasing torque disparities between $Lane_1$ and $Lane_2$ (i.e., increasing ΔT_{12}); and $Lane_1$ and $Lanes_{3\text{ and }4}$ (i.e., increasing ΔT_{13} and ΔT_{14}, where $\Delta T_{13} = \Delta T_{14}$); c) the disparities ΔT_{12}, ΔT_{13}, and ΔT_{14} were due to drift on the potentiometer in lane 1, and this should not be confused with torque disparities ΔT_{23} and ΔT_{24}, as these are purely due to inherent motor parameter disparities; and d) as the drift is limited to Pot1 only, disparities between $Lane_3$ and $Lane_4$ remain to be zero (i.e., $\Delta T_{34} = 0$).

Fig. 13b shows torque disparities due to 50 % drifts on Pot_1 and Pot_3, which has resulted in: a) a perceived increase in the positions by $Lane_2$ and $Lane_4$; b) this was accompanied by drop in the torques contributed by $Lane_1$ and $Lane_3$ (i.e., drop in T_1 and T_3), which is compensated by a rise in T_2 and T_4 to maintain a constant output torque T_{Total}; and c) this dual drift has also resulted in torque disparities between all the lanes (i. e. ΔT_{12}, ΔT_{13}, ΔT_{14}, ΔT_{23}, ΔT_{24} and ΔT_{34}). Therefore, in architectures that do not consider FE, drift in potentiometer measurements will result in increased force fight between the mismatched lanes, and therefore, the demanded aileron position will not be achieved (as shown by the curve labelled "aileron deflection" in Fig. 13b).

The response in Fig. 13c shows that architectures that consider FE will eliminate such toque disparities, regardless of the amount of drift percentage and the number of lanes affected. Therefore, Fig. 13c resembles that of Fig. 12a, demonstrating that architectures with FE offers better solutions in eliminating force fight between mismatched lanes, despite the presence of undetected drift in potentiometer readings.

7. Conclusion

This paper adds to research in the field of force equalization of torque-summed electromechanical actuators with poorly mismatched lanes. It considered a four-lanes actuation system that was designed to drive inertial and aerodynamic loads on an aileron control surface. Closed loop position control was achieved by PI with velocity feedback control action; and two types of architectures were compared. The first utilised force equalization with one common controller that reacted to the averaged fed back signals; and the second was an architecture that did not utilise force equalisation. Simulation tests considered maximum loading over a wide range of the flight envelope and included regions where the loads are purely inertial. Comparison of the two architectures revealed that while force equalisation reduced torque disparities due to high tolerance or undetected drift in one or more of the feedback transducers, it was ineffective in reducing inherent lanes disparities. Therefore, while the study demonstrated the import impact and effectiveness of this force equalisation scheme, alternative hardware compensating techniques or architectures might be necessary.

Declaration of competing interest

The authors declare that they have no known competing financial interests or personal relationships that could have appeared to influence the work reported in this paper.

References

[1] S.T. Al-Hassani, 1001 Inventions : The Enduring Legacy of Muslim Civilization, 3rd ed., National Geographic, Washington, D.C., 2012.
[2] L.J. White, Eilmer of Malmesbury, an Eleventh Century Aviator: A Case Study of Technological Innovation, Its Context and Tradition, Technol. Cult. 2 (2) (1961) 97–111.
[3] R.R. Geibert, P.B. Nolan, Kitty Hawk and Beyond: The Wright Brothers and the Early Years of Aviation: A Photographic History, Roberts Rinehart Publishers, Lanham, 2002.
[4] P. Unitt, A Dream Fulfilled: The Replica of the 1903 Wright Flyer at Wright State University, D. Dewey, Ed., Dayton, Ohio: Wright State University, 2002.

[5] F.C. Kelly, The wright brothers, A biography authorized by Orville Wright, 1st ed., Harcourt, Brace and Company inc., New York, 1943.
[6] J. P. Sutherland, "Fly by Wire: Flight Control Systems," in Proceedings of the Joint Meeting of Flight Mechanics and Guidance and Control Panels of AGARD, Oslo, 1968.
[7] V. Viswanathan, B.M. Knapp, Potential for electric aircraft, Nat. Sustain. 2 (2019) 88–89.
[8] J. B. Leonard, "A system look at the electromechanical actuation for primary flight control," in NAECON, 1983.
[9] J. B. Leonard, "A System look at Actuation Concepts and Alternatives for Primaiy Flight Control," in Proceedings of Advanced Actuation Control and Integration for Space Vehicles, Sandiego, 1985.
[10] K. Thompson, Demonstration of Electromechanical Actuation Technology for Military Air Cargo Transport, NAECON, 1983.
[11] K. Thompson, Lockheed-Georgia and Electric Primary Flight Control Systems, NAECON, 1985.
[12] K. Thomson, The Electrical Control of Large Aeroplanes, NAECON, 1987.
[13] F. Annaz, Fundamental design concepts in multi-lane smart electromechanical Actuators, Smart Mater. Struct. 14 (6) (2005) 1227–1238.
[14] K. A. Hair, "Electromechanical actuation reliability and survivability, NAECON," in NAECON, 1985.
[15] D. Ward, "The all electric helicopter," in NAECON, 1983.
[16] R. Whitaker , A. Harmon and L. Haynes, "A survivable fly-by-wire spoiler actuation system featuring non-flammable fluid, 8000 psi hydraulics and direct drive valves," in NAECON, 1985.
[17] S. C. Chenoweth, D. M. Fain and C. I. Svensson , "Redundant Actuator Development Program," Ames Research Center National Aern Autics & Space Adminstration, 1975.
[18] D.R. Ryder, Redundant actuator development study, NASA, Washington, 1973.
[19] C.C. Chenoweth, D.R. Ryder, Redundancy of Hydraulic Flight Control Actuators, Boeing Commercial Airplane Company, NASA Technical Documents, 1976.
[20] W. E. Boehringer, T. Verhoeven and W. William, "Mechanically Redundant Actuator Assembly". US Patent 5,701,801, 30 Dec 1997.
[21] Y. Zhao, W. Huang, F. Bu, Smart power flow node aimed at hybrid ac/dc power system for more electric aircraft, Electron. Lett 57 (8) (2021) 334–336.
[22] O. Mesalhy, M. Elsayed, J. Corona Jr, A. Kwarteng, Study of a high-reliability dual-fan system for cooling aerospace electromechanical actuators, Thermal Science and Engineering Progress 18 (2020).
[23] G. Bucci, F. Ciancetta, E. Fiorucci, S. Mari, Test platform for electronic control units of high-performance safety-critical multi actuator systems, International Journal of Electrical and Computer Engineering 10 (4) (2020) 4053–4072.
[24] L. Wang, J.-C. Mare, Y. Fu, Q. Haita, "Force Equalization for Redundant Active/Active Position Control System involving Dissimilar Technology Actuators," in Proceedings of the 8th JFPS International Symposium on Fluid Power, Okinawa, 2011.
[25] L. Wang, Force Equalization for Active/Active Redundant Actuation System Involving Servo-hydraulic and Electromechanical Technologies, Université de Toulouse; Institut National des Sciences Appliq, Toulouse, 2012.
[26] L. Wang, J. Maré, A force equalization controller for active/active redundant actuation system involving servo-hydraulic and electro-mechanical technologies, Proceedings of the Institution of Mechanical Engineers, Part G: Journal of Aerospace Engineers 228 (10) (2014) 1768–1787.
[27] J.R. Hoffman, Passive Load Testing for evaluation of Electromechanical Actuators, Air Force Institute of Technology, March 2018.
[28] D. Wroble, Force Fight Study in a Dual Electromechanical Actuator Configuration, University of Dayton, Dayton, 2017.
[29] D. Y. Wang, D. Q. Li, J. Chen and S. C. Zheng, "A Position Synchronization Control for Dual Redundant Electro-Mechanical Actuation in Flight Control System," in IOP Conf. Series: Materials Science and Engineering, 2019.
[30] W. Rehman, X. Wang, S. Wang and I. Azhar, "Motion Synchronization of HA/EHA System for a Large Civil Aircraft by Using Adaptive Control," in IEEE Chinese Guidance, Navigation and Control Conference, Nanjing,China, 2016.
[31] F. Annaz, Worthy Test Programs and Developments in Smart Electromechanical Actuators, Smart Mater. Struct. 16 (2007).
[32] F. Annaz, Design and Development of Multi-Lane Smart Electromechanical Actuators, IET, 2014.
[33] Mil-F-83300, Flying qualities of piloted VSTOL aircraft, 1970.
[34] Mil-C-18244, Flying qualities of piloted VSTOL aircraft, 1970.
[35] I. M. D. Publication, "Kollmorgen SILVERLINETM Brushless Series Motors," Kollmorgen Motion Technologies Group, 1989. [Online]. Available: https://www.kollmorgen.com/sites/default/files/public_downloads/Silverline%20Motor%20Catalog.pdf. [Accessed 01 May 2023].
[36] kollmorgen, "kollmorgen: aerospace and defense," [Online]. Available: https://www.kollmorgen.com/en-us/solutions/aerospace-and-defense/aerospace-defense/. [Accessed 01 May 2023].
[37] M. I. Research, "Rotary Variable Differential Transducer," 2019. [Online]. Available: https://www.mtcind.com/mtc-rvdt-116. [Accessed 01 May 2023].
[38] M. Inc., "Rotary Variable Differential Transformer (RVDT," 2019. [Online]. Available: https://www.moog.com/literature/MCG/RVDTDtS.pdf. [Accessed 01 May 2023].